ORIGINAL PAPER

Mechanical properties of non-cohesive polygonal particle aggregates

Pradip Roul · Alexander Schinner · Klaus Kassner

Abstract We numerically investigate the effective material properties of aggregates consisting of soft convex polygonal particles, using the discrete element method. First, we construct two types of "sand piles" by two different procedures. Then we measure the averaged stress and strain, the latter via imposing a 10% reduction of gravity, as well as the fabric tensor. Furthermore, we compare the vertical normal strain tensor between sand piles qualitatively and show how the construction history of the piles affects their strain distribution as well as the stress distribution. In the next step, elastic constants are determined, assuming Hooke's law to be locally valid throughout the sand piles. We determine the relationship between invariants of the stress and strain tensor, observing that the behaviour is nonlinear. While linear elastic behaviour near the centre of the pile is compatible with our data, nonlinearity signals the transition to plastic behaviour near its surface. A similar behaviour was assumed by Cantelaube et al. (Static multiplicity of stress states in granular heaps. Proc R Soc Lond A **456**:2569–2588, 2000). We find that the macroscopic stress and fabric tensors are not collinear in the sand pile and that the elastic behaviour is anisotropic in an essential way.

Keywords Sand pile · Stress · Strain · Fabric · Discrete element method

P. Roul (✉) · K. Kassner
Institute of Theoretical Physics, Otto-von-Guericke University
Magdeburg, Postfach 4120, 39106 Magdeburg, Germany
e-mail: pradip.roul@uni-due.de

P. Roul
Institute for Numerical Mathematics, Duisburg-Essen University,
47058 Duisburg, Germany

A. Schinner
T-Systems, Dachauer Straße 665, 80995 München, Germany

1 Introduction

In the last few years, extensive research has been devoted to the study of granular materials due to their importance for applications in various industries. Moreover, they pose fundamental analytical challenges [1,2]. An important issue is to understand how the mechanical properties of granular matter arise, both in dynamic configurations and in the static limit. In this regard, one of the simplest examples out of a collection of possible granular arrangements is the static sand pile, and the practical issue of storing granular materials in the form of sand piles occurs in many industrial situations. In order to handle the processing of granular material in a sand pile properly, it is useful to understand its mechanical properties and effective material behaviour.

The stress distribution under a heap of sand displays some interesting properties [3–6] which may be traced back to the static indeterminacy of friction-stabilized aggregates. This has led to a multitude of studies concerning the pressure or stress distribution beneath sand piles under a large variety of conditions [7–21]. Depending on characteristics such as the size and shape distribution of particles but also the construction history of the aggregate, piles consisting of the same material may have different stress distributions [6]. If the pile is created by dropping material from a point source (*wedge sequence* [22]), there usually is a stress minimum below the centre of the pile, while if it is dropped layer-wise (*layered sequence* [23]), there is no minimum in the vicinity of the centre. For a detailed description of the practical realization of wedge and layered sequences, see Ref. [23]. In some cases, the stress distribution displays a pronounced minimum below the tip of the sand pile and in others the minimum is only a weak indentation [9]. If the sand pile contains a mixture of ellipsoidal particles, a large stress dip appears below the tip of the pile for a certain construction history of the pile, whereas

when it contains a mixture of roundish particles, there is a much smaller dip [9,10].

To a certain extent, even more interesting than studying the stress tensor is to determine the strain distribution within a sand pile. One might regard it as one of the essential questions in the discussion of granular heaps, whether and how deformation fields in the presence of stress can be defined; such a question aims at the identification of a strain tensor and at establishing a correlation between the stress and strain tensors, in order to determine effective material properties. Up to now, strains have not been measured in experiments on sand piles, nor is there any discussion, how such a feat might be accomplished. Theoretical models and analysis assume that for sand piles displacement fields are not available. Therefore, constitutive relations proposed for sand piles [1,2] have been obtained without the introduction of a strain tensor. Of course, one may wonder whether the notion of a constitutive relation makes sense at all, if the behaviour of the system is history dependent, i.e., if the system does not have a state in the sense of the original meaning of the word, referring to a situation characterized by a few state variables, no matter how these were prepared. To some extent, speaking of a state and of constitutive relations describing the way state variables are connected with each other, excludes history dependence! On the other hand, there is a well-known example where this kind of language is used nevertheless, and where it works well: this is the case of a ferromagnet. A given external field does not uniquely determine the magnetization of a ferromagnetic system, which in addition depends on how the preceding state was arrived at, whether the field was reduced to its current value from above or increased from below, and so on. Nevertheless, one can define constitutive relations for ferromagnetic states either by specifying them for incremental state changes or by giving full magnetization curves for a preparation history starting from a well-defined initial state.

If we hypothesize that the situation for a sand pile is similar, knowing that there is a history dependence but also that states with a controlled history are reproducible, it is meaningful to ask both the question of sensitivity to preparation procedures and whether the usual conjugate variable to stress, which is strain, can be a significant element in the description of a sand pile in terms of a constitutive relation, presumably with restrictions applying, concerning the range of such a relation or its integrability.

In this paper, we focus, on the one hand, on the sensitivity of the strain distribution to the preparation of sand piles; on the other hand, we wish to investigate numerically the effective material properties of sand piles. By performing simulations in the framework of a discrete element method (DEM), we obtain a macroscopic strain tensor from microscopic quantities, *viz.* the displacements of the individual grains in a two-dimensional sand pile. Then we can estimate local elastic coefficients assuming Hooke's law. Generally speaking, if we find almost constant values for the macroscopic elastic coefficients throughout the sand pile, linear elasticity may be considered a good approximation. If we obtain, however, strongly varying elastic coefficients, then we can say that linear elasticity does not work for the pile as a whole. In addition, this computation will serve as a consistency check for theoretical assumptions such as the rigid-particle hypothesis. If our calculation produced macroscopic elastic constants of the same order of magnitude as the microscopic Young's modulus Y that we assign to the particles for the calculation of forces (explained below), then the idea that the sand pile has a macroscopic elastic behaviour different from that of its microscopic constituents would be invalidated, and the elastic moduli of the pile would go to infinity with those of the grains. This idea can work only, if the sand pile admits a finite elastic response in spite of the rigidity of the grains, which means that elastic coefficients such as the *macroscopic* Young's modulus E of the sand pile must be significantly smaller in the simulation than those of the particles. In non-cohesive media elastic coefficients such as E can describe responses to compressive stresses only, as tensile stresses are not supported by the material. Hence the notion of elasticity has a more restricted meaning than usual.

The paper is organized as follows. In Sect. 2, we first describe our simulation method for two-dimensional "sand piles" consisting of soft convex polygonal particles. In Sect. 3, we determine the stress tensor as well as the strain tensor, adopting Cambou's best-fit strain approach for the latter. We discuss the averaging procedure used to extrapolate to macroscopic fields. Then we present simulation results for averaged vertical normal strains at different heights inside a sand pile poured from either a point source or a line source. We introduce the fabric tensor of polygonal particles and discuss the properties of its macroscopic average in Sect. 4. Once the (incremental) stress and strain tensors are determined, we calculate macroscopic elastic coefficients assuming Hooke's law of (anisotropic) linear elasticity in Sect. 5. Section 6 discusses stress and strain invariants. Conclusions are drawn in Sect. 7.

2 Simulation method

We perform numerical simulations, in which a sand pile is constructed from several thousand convex polygonal particles with varying shapes, sizes and edge numbers. The particles are poured from either a point source, i.e. according to the wedge-sequence protocol, which regularly leads to a pressure minimum under the pile, or from a line source, with the length of the line being continuously adapted to the momentary width of the top of the pile, which corresponds to the layered-sequence protocol [23]. We use a discrete-element method with soft but shape invariant particles:

two particles in contact with each other are allowed to inter-penetrate partially. It would be inefficient to solve the elastic equations for each collision between pairs of nonrigid particles, so we do not allow shape changes. An alternative approach allowing the (desirable) solution of the equations of motion for rigid particles would be contact dynamics [24–26], which is algorithmically very demanding and does not scale linearly with the particle number. Event-driven codes [27,28] could in principle also realize rigid particles, but this would be too cumbersome with polygonal particles. Moreover, event-driven simulations become inefficient in the limit of large densities (due to the phenomenon of inelastic collapse). Therefore, small overlaps of particles are accepted, but a repulsive force is introduced that is proportional to the overlap area.

We solve the equations of motion following from the balances of momentum and angular momentum for each particle, using a fifth-order Gear predictor-corrector method [29]. Forces between colliding particles are calculated from the geometric characteristics of the overlap area and contact length (defined in the appendix) and the relative velocities of the two particles. A brief description is given in the appendix. The calculation involves phenomenological elastic constants such as the particle Young's modulus Y as well as model parameters for friction and viscous damping. Details on the verification of the model assumptions concerning the realization of static friction and the avoidance of unphysical oscillations are given in [30], a description of algorithmic tricks to speed up collision detection is presented in [31].

In two dimensions, there are three quantities per particle, characterizing its position (two coordinates) and its orientation (one angle); for these, the momentum balance provides two equations, the angular momentum balance another one:

$$m_i \ddot{\mathbf{r}}_i = \sum_{j=1}^{n(i)} \mathbf{F}_{ij} + \mathbf{G}_i, \quad I_i \ddot{\varphi} = \sum_{j=1}^{n(i)} L_{ij}. \tag{1}$$

Here, the subscript i runs over all the particles and the subscript j over all the contacts of particle i with other particles. That is, forces and torques are exchanged between particles only if they touch each other. Hence we have contact forces and these are short range. $\mathbf{G}_i$ is the force acting on particle i due to external fields, in our case just gravity, $\mathbf{F}_{ij}$ the force created by the particle touching particle i in contact j. There is at most one contact between two particles as our polygons are restricted to being convex.

The force calculation is one of the most time-consuming parts of the algorithm. Of course, advantage is taken of the short-range nature of the forces by calculating only non-vanishing forces, i.e., forces between particles that are really in contact with each other. To achieve fast contact determination in a time that is proportional to the number of particles

(not to its square), independent of the complexity, i.e., the number of edges of the particles, algorithms from virtual reality and computational geometry were adapted. These use bounding boxes and Voronoi regions to determine overlaps of particles [30,31].

3 Stress and strain calculations

From the forces, we can compute stresses by appropriate averaging procedures. It is easy to derive a formula for the average stress obtained in a homogeneous polygonal particle [32], assuming that the forces given in the contact points act on the corresponding edge of the polygon:

$$\sigma_{ij}^p = \frac{1}{V^p} \sum_{c=1}^{m} x_i^c f_j^c, \tag{2}$$

where x_i^c is the ith component of the branch vector pointing from the centre of mass of the particle to the contact point c, and f_j^c is the jth component of the total force in that contact point. V^p is the volume of particle p (actually its area, since we are working in 2D).

Expression (2) may be interpreted as the stress tensor associated with a single particle. This microscopic stress would not be a convenient means to describe the macroscopic sand pile, as it fluctuates wildly within a volume containing a few sand grains. Moreover, it is not defined in the voids between the grains. Hence, for a continuum description, we need to average microscopic stresses. Weighting each particle with its volume fraction the prefactor $\frac{1}{V^p}$ in Eq. 2 gets replaced by $\frac{1}{V}$ and a sum over all particles (i.e. over p) is performed (see for example [33]).

A representative volume element (RVE) is introduced via the requirement that the average becomes size independent, if the volume is taken equal to this value or larger. Averaging over different volumes gives different results, as long as the volume element is too small. As we increase the size of the volume element in the computation of the average, the latter converges to a certain value as shown in Fig. 1. We find that sizes of the volume element containing 100–200 particles are sufficient to serve as RVE.

While the calculation of stresses is rather straightforward, this is not true for strains. In fact, even the definition of strain is problematic after assuming particles to be essentially rigid. For this reason, most macroscopic descriptions proposed in the last few years try to get by without using strain at all. Whether this approach can be successful in the long run remains to be seen. In any case, even if it may be difficult or impossible to determine strains in *experiments* on sand piles, this is not quite so in a *simulation*.

Our original idea was to define strains with respect to a hypothetical reference state of zero gravity of a sand pile
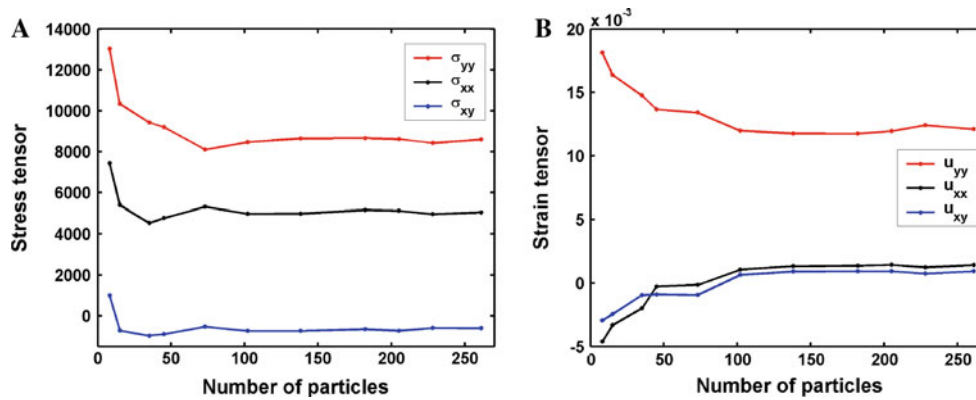
Fig. 1 Convergence behaviour of **a** the stress tensor components, **b** the strain tensor components, as the number of particles in the volume element used for averaging is increased. Obviously, the RVE should be chosen to contain at least 100 particles. The stress tensor is given in units N/m, the strain tensor is nondimensional

essentially identical to the one at ambient gravity, except of course for slightly displaced particle centres. In this reference state, no particle rearrangements should be present in comparison with the actual state. The reference state would then be obtained from the ambient one by slowly reducing gravity. In principle, it is not necessary to go down to zero gravity, as long as the strains increase linearly with the gravity level—one may then extrapolate to zero from the knowledge of the positions of the particle centres of mass at two arbitrary different gravity levels. Of course, it is necessary to let the sand pile approach a state of rest after a reduction of gravity. Moreover, linearity has to be checked by looking at different changes of gravity level.

This method does not work as expected, as we found out by doing the measurements in simulations, since a reduction of gravity leads to a proportional reduction only of normal stresses corresponding to the direction of gravity, i.e. of σ_{yy}, but not of σ_{xx}. Stresses in the x direction are essentially due to static friction of the pile with its support. Since most contacts are not fully mobilized, contact forces at the bottom of the pile are not strictly proportional to the normal force (their weight); the effective friction coefficient can vary between 0 and μ during a change of the gravity level. Hence, the method does not yield absolute displacements, as we have no access to the hypothetical reference state. Nevertheless, it is of course still possible to determine incremental strains, which are defined as the strain changes between the actual state and a state at a different gravity level. Using incremental stresses as well, we are then in a position to determine macroscopic elastic coefficients.

We are aware of two approaches given in the literature for determining averaged strains in an assembly of grains, the equivalent continua theories [34,35] and the least-square fit theories [36]. In our study, we use one of the simplest

techniques, namely the best-fit strains of Cambou et al. [36] who consider the relative translation instead of the contact deformations, which means to exclude particle rotations from the analysis. Displacements are characterized in terms of the translations of the particle centres.

Let du_i^p denote the translation of the centre of particle p along axis i [$i = x \;(\stackrel{\triangle}{=} 1)$ or $i = y(\stackrel{\triangle}{=} 2)$]. The relative translation of the pairs of grains p and q forming contact c is

$$d\Delta u_i^c = du_i^q - du_i^p \tag{3}$$

If every particle of an assembly of grains moved according to a uniform displacement gradient tensor ε_{ji}, then the relative translation at contact c would be

$$d\Delta u_i^c = \varepsilon_{ji} l_j^c \tag{4}$$

where l_j^c is the j compoent of the vector joining the centres of mass of the two particles sharing contact c and we have used the Einstein summation convention for repeated subscripts. Whenever a pair of subscripts arises in a product or at a single tensor, summation over this subscript is implied (unless it is explicitly excluded in the accompanying text).

However, usually microscopic displacements do not normally have uniform gradients, so for a general case, we would have

$$d\Delta u_i^c \neq \varepsilon_{ji} l_j^c \tag{5}$$

Then, we determine the tensor ε_{ji} for which the square sum of the deviations in (5) is smallest i.e, we minimize the following quantity

$$Z = \sum_c (d\Delta u_i^c - \varepsilon_{ji} l_j^c)^2. \tag{6}$$

with respect to ε_{kl}, i.e., we set $\frac{\partial Z}{\partial \varepsilon_{kl}} = 0$ for every pair k, l.
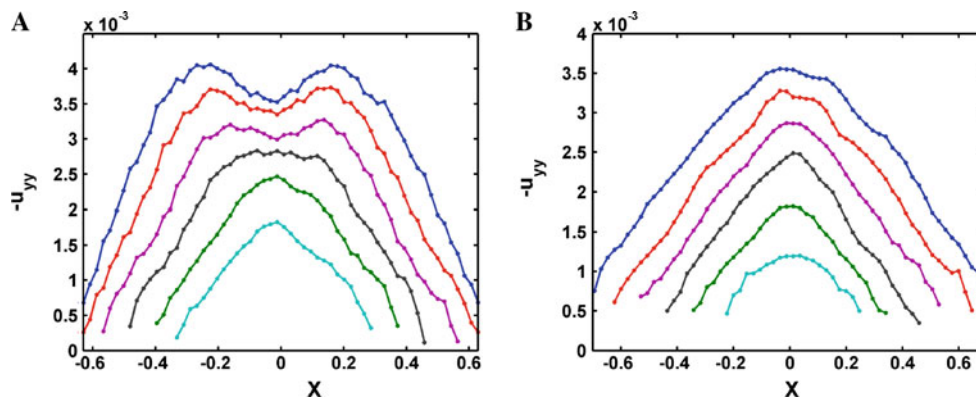
Fig. 2 Vertical normal strain distribution at different heights of simulated sand piles. **a** sand piles constructed using wedge sequences (average over 9 piles), **b** sand piles poured in layered sequences (average over 10 piles). Height levels: 4.5, 9, 13.5, 18, 22.5, 27 cm. The curve with the largest lateral extension corresponds to the lowest height level, the one with the smallest extension to the top level. The length unit of the abscissa is 1 m

Equation 6 gives four equations in 2D which can be written in matrix form as follows

$$\begin{pmatrix} \sum\limits_{c=1}^{n} l_1^c l_1^c & \sum\limits_{c=1}^{n} l_2^c l_1^c \\ \sum\limits_{c=1}^{n} l_1^c l_2^c & \sum\limits_{c=1}^{n} l_2^c l_2^c \end{pmatrix} \begin{pmatrix} \varepsilon_{1i} \\ \varepsilon_{2i} \end{pmatrix}$$

$$= \begin{pmatrix} \sum\limits_{c=1}^{n} d\Delta u_i^c l_1^c \\ \sum\limits_{c=1}^{n} d\Delta u_i^c l_2^c \end{pmatrix} (i \text{ is 1 or 2}) \quad (7)$$

The coefficient matrix on the left-hand side of (7) is positive definite, if there exist at least two branch vectors in the system that are not parallel to each other. This is the necessary and sufficient condition of the existence of the Cambou et al. best-fit strain in 2D.

Let z_{ij} denote the inverse of the coefficient matrix. In order to determine the ε_{11} and ε_{21} we substitute $i = 1$, whereas $i = 2$ is substituted for the calculation of ε_{12} and ε_{22}. The solution of (7) can be written in the general form

$$\varepsilon_{ij} = z_{ik} \sum_c d\Delta u_j^c l_k^c \quad i, j = 1, 2 \quad (8)$$

The tensor ε_{ij} in (8) is the best-fit translation gradient of Cambou et al. [36]. The components of the strain tensor in two dimensions are as follows

$$\varepsilon_{xx}(x, y) = \sum_c d\Delta u_x^c \left(z_{11} l_x^c + z_{12} l_x^c \right), \quad (9a)$$

$$\varepsilon_{yy}(x, y) = \sum_c d\Delta u_y^c \left(z_{21} l_y^c + z_{22} l_y^c \right), \quad (9b)$$

$$\varepsilon_{xy}(x, y) = \sum_c d\Delta u_y^c \left(z_{11} l_x^c + z_{12} l_x^c \right), \quad (9c)$$

$$\varepsilon_{yx}(x, y) = \sum_c d\Delta u_x^c \left(z_{21} l_x^c + z_{22} l_y^c \right). \quad (9d)$$

The box size used for the computation of the strain tensor is the same as for the stress tensor. It may be added that we also have determined strains by direct numerical differentiation and compared these displacement gradients with various strain definitions from the literature, including the Cambou strain. It turns out that the Cambou strain is closest to the displacement gradient and numerically well-behaved even near the sandpile surface, where fluctuations render numerical differentiation awkward.

Being essentially a displacement gradient, the Cambou strain is not necessarily symmetric. We will denote symmetrized strains by u_{ij}, i.e. $u_{xy} = \frac{1}{2}(\varepsilon_{xy} + \varepsilon_{yx})$, whereas there is no difference between u_{ij} and ε_{ij} when $i = j$.

3.1 Simulation results

In all the simulations discussed in this article, the particles were polygons inscribed into an ellipse with a corner number randomly chosen between 6 and 8. The particle size varied by 30% about an average value of 3.4 mm for both the semi-major and semiminor of the ellipse, which were drawn from a uniform random distribution.

The vertical normal strain tensor component obtained from DEM simulations is displayed in Fig. 2 for sand piles that were constructed using the two different pouring protocols wedge sequence and layered sequence. The averaged strain tensor was evaluated throughout the sand pile; we represent it via a plot of tensor components as a function of the lateral coordinate x of the pile for layers of given heights $y_1, y_2, \ldots, y_n$.

We give this component of the strain tensor to obtain a qualitative picture, although the foregoing discussion shows that it is not a rigorously determined quantity. While it has the correct scaling with gravity, vertical and horizontal strains are of course coupled, so the errors produced by the method in the horizontal direction will also affect the vertical direction. The

topmost curve in the graph shows the strain tensor result at the bottom layer of the corresponding sand pile, whereas the bottom curve corresponds to the top layer.

An interesting feature of the vertical normal strain tensor for various heights is that the vertical normal strain changes with the layer position in the sand piles like the stress tensor. The vertical normal strain shows a dip (Fig. 2a) near the centre of the piles that are poured from a point source, i.e., according to the wedge-sequence protocol. It can be seen that the strain dip appears not only at the bottom layer but also exists up to a certain height of the sand pile. For sand piles poured as layered sequences, the vertical normal strain increases towards the centre and towards the bottom layer of. A strain dip does not occur in the profiles of these sand piles, constructed from a line source.

4 Fabric tensor

The density distribution is not homogeneous under a sand pile that is poured from a point source. Therefore, the internal texture of the pile is an important quantity. Furthermore, forces are propagated from one particle to the neighbour particles in an assembly of grains only via the contact points of the particle. Thus, for the quasi-static mechanics of granular aggregates, it is useful to have a description of the associated contact network of the inter-particle contacts.

A particular quantity used to characterize the internal texture of the granular assembly is the so-called fabric tensor [37,38]. Various definitions of the fabric tensor exist in the literature including definitions for elliptical, spherical or polygonal particles. In our study, we consider non-spherical particles so we employ here a mathematical formulation for the fabric tensor, in which the branch vector itself is used to define a unit vector in the direction towards the contact, because the simplest way of characterizing the packing network is via the branch vectors connecting the particle centres of mass with their contact points.

Once we have the contact points of the individual particles, we can calculate a fabric tensor for each particle, which yields an additive contribution to the overall fabric tensor. The latter then is a volume average over many particles. After defining the fabric tensor for one particle and for an aggregate of grains, we will demonstrate how it may be used to examine the granular structure of a material for isotropy. The fabric tensor relates the contact number density in the assembly to directional information. Therefore, it may be used to examine whether there exists any directional ordering in the material. Our nomenclature and definitions relating to the fabric tensor closely follow the work of Luding [33,39,40]. Moreover we are interested in the same quantities obtainable from the fabric tensor as the authors of [33,39,40].

4.1 The fabric tensor for one particle

The general formula for the fabric tensor of a single particle is given [37,38] by

$$F_{ij}^p = \sum_c n_i^c n_j^c, \tag{10}$$

where n_i^c is the ith component of the unit vector from the centre of mass of the considered particle p to its contact point c with another particle and the sum is over all contacts:

$$
\begin{aligned}
n_1^c &= \frac{x_c - x_p}{\sqrt{(x_c - x_p)^2 + (y_c - y_p)^2}}, \\
n_2^c &= \frac{y_c - y_p}{\sqrt{(x_c - x_p)^2 + (y_c - y_p)^2}}.
\end{aligned}
\tag{11}
$$

Herein, (x_c, y_c) and (x_p, y_p) are the contact point and the centre of mass, respectively. The trace of the single-particle fabric tensor is equal to the number of contacts of particle p:

$$tr(F_{ij}^p) = \sum_{c,i} n_i^c n_i^c = C^p. \tag{12}$$

(Here, the Einstein summation convention was not applied.) We take an average weighted by the volume of the particles over many particles within a representative volume element in order to determine the average fabric tensor describing the contact network in a given volume V [33,40].

4.2 Properties of the fabric tensor

The fabric tensor is symmetric by definition and therefore normally consists of three independent components in two dimensions. These may be expressed in a coordinate independent way using tensor invariants and geometrical quantities.

As the first of these quantities, we choose the trace of the fabric tensor, which is a scalar. It is also known as the volumetric part of the fabric and given by $tr(F) = F_{max} + F_{min}$, where F_{max} and F_{min} are the major and minor eigenvalues of the fabric tensor, respectively. In Fig. 3a, the trace of the averaged fabric tensor is plotted at different heights inside the sand pile. It can be seen from the figure that the mean number of contacts decreases near the surface of the sand pile and increases with increasing distance from the surface to the centre of the sand pile. Since we have measured the density to increase towards the centre of the pile in the case of a pile poured from a point source, this means that the number of contacts is higher where the density is larger (although the pressure is lower in the bottom layers).

As a second independent quantity determining the fabric tensor we may choose the fabric deviator. It is defined as $F_D = F_{max} - F_{min}$ and is a measure of the degree of anisotropy in the contact network of the granular assembly. The
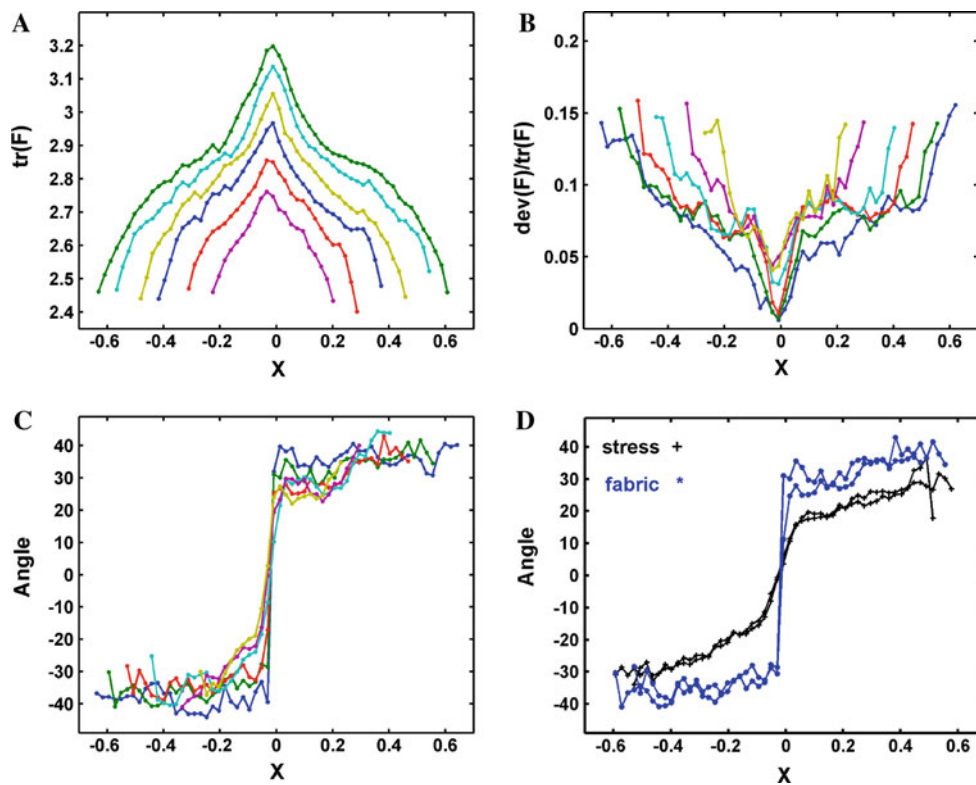
Fig. 3 **a** Trace of the fabric tensor, **b** deviatoric fraction, **c** orientation of fabric versus lateral position in the sand pile, and **d** orientation of fabric, stress and strain plotted only for the first two bottom layers of the pile. The sand piles were produces by wedge sequences. Length units are as in Fig. 2, angles are given in degrees

deviatoric fraction of the fabric tensor $F_D/tr(F)$ is plotted in Fig. 3b for different heights inside the sand pile. From the figure, it is observed that the deviatoric fraction decreases towards the centre. This means that the fabric is more isotropic near the centre of the sand pile and more anisotropic in the outer part. The fabric anisotropy is between 0 and 0.15.

The angle of orientation of the major eigenvector of the fabric tensor may serve as the third independent quantity defining the fabric tensor. The orientation of the major eigenvector with respect to the vertical axis is given in Fig. 3c at different heights inside the sand pile. It changes from −40 degrees (left) to +40 degrees (right).

The orientation of the macroscopic tensors stress and fabric are plotted in Fig. 3d only for the first two bottom layers of the pile. We omit the strain tensor, since the xx and xy components of the former cannot be determined reliably. It can be seen, however, that the orientations are different for the fabric and stress tensors, which means that these macroscopic tensors are not collinear. Most likely this limits the utility of a description of granular piles in terms of isotropic elasticity. Nevertheless, we shall consider such a description in the following as well as one in terms of anisotropic elasticity to explore these limitations in some detail. In particular, since along the central line of the sand pile the fabric tensor

is almost isotropic, the determination of the orientation of its principal axes is necessarily of lower precision than outside the central interval $x \in [-0.1\text{m}, 0.1\text{m}]$. An almost isotropic situation is therefore not excluded near the centre of the pile and it is indeed assumed in some theories [1,18].

5 Determination of macroscopic elastic constants

Having determined the stress tensor and strain tensor we can obtain the effective material properties of sand piles assuming Hooke's law. This should be considered a tentative approach. It does not mean that we believe Hooke's law to be valid throughout the sand pile. In fact, we have shown in a preceding paper [41] that the elastoplastic approach by Cantelaube et al. [1,18] is surprisingly good, describing the pressure distribution of layered sand piles well without adjusting any parameters, whereas it gives a decent approximation to sand piles with a pressure minimum after adjusting a single parameter. Hence, at least near the surface of the pile, a purely elastic description must fail. However, the calculation of elastic coefficients will provide us with two pieces of information. On the one hand, it is important to know whether the sand pile has elastic properties beyond those of its constituent particles

(given by the fixed microscopic Young's modulus Y assigned to each particle), that is, would there still be an elastic-like response of a sand pile, if it consisted of rigorously rigid particles? A necessary prerequisite for answering this question in the affirmative is that the macroscopic elastic coefficients obtained for the pile are substantially below those with which the particles have been endowed for the purpose of numerical simulation. On the other hand, we can push the comparison with elastoplastic theory further to find out whether it describes the stress distribution in the whole pile well, not just at its bottom.

In linear elasticity, there is an elastic potential

$$W = \frac{1}{2}\lambda_{ijkl}u_{ij}u_{kl}, \tag{13}$$

leading to the general stress-strain relationship (Hooke's law) [42]

$$\sigma_{ij} = \lambda_{ijkl}u_{kl}, \tag{14}$$

where the λ_{ijkl} are the elastic moduli constituting the stiffness tensor. The symmetry of the stress and strain tensors and the existence of an elastic potential give rise to a reduction of the number of independent components of the stiffness tensor. In two dimensions, instead of $2^4 = 16$, only 6 of its elements are independent. In explicit form, the elastic law reads

$$\begin{aligned}
\sigma_{xx} &= \lambda_{xxxx}u_{xx} + \lambda_{xxyy}u_{yy} + 2\lambda_{xxxy}u_{xy}, \\
\sigma_{yy} &= \lambda_{xxyy}u_{xx} + \lambda_{yyyy}u_{yy} + 2\lambda_{xyyy}u_{xy}, \\
\sigma_{xy} &= \lambda_{xxxy}u_{xx} + \lambda_{xyyy}u_{yy} + 2\lambda_{xyxy}u_{xy}.
\end{aligned} \tag{15}$$

Thanks to linearity, this law holds for incremental stresses and strains as well, if it does for total stresses and strains. We measure incremental stresses and strains at many points inside the pile. Then we can construct a sum

$$\begin{aligned}
S(x, y) = \sum_{r=1}^{m}&\left(\sigma_{xx}^{(r)} - \lambda_{xxxx}u_{xx}^{(r)} - \lambda_{xxyy}u_{yy}^{(r)} - 2\lambda_{xxxy}u_{xy}^{(r)}\right)^2 \\
&+ \left(\sigma_{yy}^{(r)} - \lambda_{xxyy}u_{xx}^{(r)} - \lambda_{yyyy}u_{yy}^{(r)} - 2\lambda_{xyyy}u_{xy}^{(r)}\right)^2 \\
&+ 2\left(\sigma_{xy}^{(r)} - \lambda_{xxxy}u_{xx}^{(r)} - \lambda_{xyyy}u_{yy}^{(r)} - 2\lambda_{xyxy}u_{xy}^{(r)}\right)^2
\end{aligned} \tag{16}$$

where the superscript r runs over a number m of data points measured in the close vicinity of the coordinate pair (x, y). We usually take them near the centre of the RVE used in the evaluation of the tensor fields. Then S is minimized with respect to the elastic moduli λ_{ijkl} which produces a least-squares approximation to these parameters. Ordinarily, we obtain six equations for the six moduli at each point (x, y). For the sake of accuracy and in order to obtain easily interpretable elastic coefficients, we modify and simplify the procedure a little.

We can determine the stress tensor components more accurately than those of the strain tensor, because we either have to compute numerical derivatives for the latter or to use a fitting procedure [36], whereas the stress tensor is obtained by straightforward averaging. Hence, it is more useful to start from the inversion of (14),

$$u_{ij} = s_{ijkl}\sigma_{kl} \tag{17}$$

where s_{ijkl} is the compliance tensor and to define an analogous sum $\tilde{S}(x, y)$ containing the expressions from the inverted version of Hooke's law in squared parentheses. Just as the number of strain terms in S is three times larger than the number of stress terms, the number of stress terms in $\tilde{S}$ is three times larger than that of strain terms. Moreover, because interpretation of the results is somewhat cumbersome with six different elastic coefficients, we restrict ourselves to the two simplest cases, that of cubic anisotropy and the isotropic case. Abbreviating s_{xxxx}, s_{xxyy}, and s_{xyxy} by s_1, s_2, and s_3, respectively, we have for the sum of squares that is to be minimized with respect to the s_i:

$$\begin{aligned}
\tilde{S}(x, y) = \sum_{r=1}^{m}&\left(u_{xx}^{(r)} - s_1\sigma_{xx}^{(r)} - s_2\sigma_{yy}^{(r)}\right)^2 \\
&+ \left(u_{yy}^{(r)} - s_2\sigma_{xx}^{(r)} - s_1\sigma_{yy}^{(r)}\right)^2 + 2\left(u_{xy}^{(r)} - s_3\sigma_{xy}^{(r)}\right)^2.
\end{aligned} \tag{18}$$

Introducing the notation $\langle A \rangle = \frac{1}{m}\sum_{r=1}^{m}A^{(r)}$, the solution of this minimization problem is given by

$$s_1 + s_2 = \frac{\langle(u_{xx} + u_{yy})(\sigma_{xx} + \sigma_{yy})\rangle}{\langle(\sigma_{xx} + \sigma_{yy})^2\rangle}, \tag{19}$$

$$s_1 - s_2 = \frac{\langle(u_{xx} - u_{yy})(\sigma_{xx} - \sigma_{yy})\rangle}{\langle(\sigma_{xx} - \sigma_{yy})^2\rangle}, \quad s_3 = \frac{\langle u_{xy}\sigma_{xy}\rangle}{\langle\sigma_{xy}^2\rangle},$$

and the elastic moduli are obtained from

$$\begin{aligned}
\lambda_{xxxx} \equiv \lambda_1 = \frac{s_1}{s_1^2 - s_2^2}, \quad \lambda_{xxyy} \equiv \lambda_2 = \frac{-s_2}{s_1^2 - s_2^2}, \\
\lambda_{xyxy} \equiv \lambda_3 = \frac{1}{2s_3}.
\end{aligned} \tag{20}$$

The isotropic limit corresponds to $\lambda_3 = G = \frac{1}{2}(\lambda_1 - \lambda_2)$. In this case, the sum S may be replaced by

$$\begin{aligned}
S' = \sum_{r=1}^{m}&\left[(\sigma_{xx}^{(r)} + \sigma_{yy}^{(r)}) - 2K(u_{xx}^{(r)} + u_{yy}^{(r)})\right]^2 \\
&+ \left[(\sigma_{xx}^{(r)} - \sigma_{yy}^{(r)}) - 2G(u_{xx}^{(r)} - u_{yy}^{(r)})\right]^2 \\
&+ 4\left[\sigma_{xy}^{(r)} - 2Gu_{xy}^{(r)}\right]^2, \tag{21}
\end{aligned}$$

a case in which we can directly minimize with respect to the bulk modulus K and the shear modulus G.

This leads to

$$K = \frac{\langle (\sigma_{xx} + \sigma_{yy})(u_{xx} + u_{yy}) \rangle}{2 \langle (u_{xx} + u_{yy})^2 \rangle},$$

$$G = \frac{\langle (\sigma_{xx} - \sigma_{yy})(u_{xx} - u_{yy}) \rangle + 4 \langle \sigma_{xy} u_{xy} \rangle}{2 \left(\langle (u_{xx} - u_{yy})^2 \rangle + 4 \langle u_{xy}^2 \rangle \right)}.$$

Note that we assume *local* isotropy only when evaluating the bulk and shear modulus this way. Globally, the system can be anisotropic similar to a liquid under hydrostatic pressure, where the up-down direction clearly is distinguished. From (22), we can calculate the macroscopic Young's modulus via $E = 3G - \frac{G^2}{K}$.

In order to compare isotropic elasticity with the case of cubic anisotropy, we calculate the bulk modulus and versions of Young's modulus and the shear modulus for that case, too. The bulk modulus is direction independent and simply given by $K = \frac{1}{2}(\lambda_1 + \lambda_2)$. Young's modulus is orientation dependent. Along the x and y axes, it takes the value $E_p = (\lambda_1^2 - \lambda_2^2)/\lambda_1$, along the bisectors (at angles of 45°), $E_b = \lambda_1 + \lambda_2$. The average of the two quantities is $E_{av} = \lambda_1 + \frac{1}{2}(\lambda_1 - \lambda_2)\lambda_2/\lambda_1$. For the shear modulus along the principal directions, we find $G_p = \lambda_3$, for the shear modulus along the bisectors $G_b = \frac{1}{2}(\lambda_1 - \lambda_2)$, hence the average over these two directions is $G_{av} = \frac{1}{2}\lambda_3 + \frac{1}{4}(\lambda_1 - \lambda_2)$. Figure 4 gives some results from calculations along these lines.

In the figure, we compare straightforward calculations assuming isotropic linear elasticity with averages over two nonequivalent orientations (chosen parallel to the x or y axes and to their bisector) from calculations for linear elasticity with cubic (or rather, square, since everything is 2D) anisotropy. Let us focus first on the bulk modulus and Young's modulus. We note that the two calculations give very similar results, meaning that the assumed anisotropy has little effect on these two elastic constants. This is not due to orientation averaging in the case of Young's modulus, as this elastic constant is almost the same for the two nonequivalent orientations. (The bulk modulus is isotropic, so it was not orientationally averaged.)

There are some differences between the left-hand side pictures and those on the right-hand side, though, even for these two moduli. When fitting moduli (according to the formulas for S or S'), we find that the resulting elastic coefficients go to zero near the surface of the pile. This is also true for the anisotropic case as we have verified but do not show here. When fitting compliances (according to the formula for $\tilde{S}$), the resulting moduli remain finite near the surface at least in the lower layers, and the curves are smoother for lower layers but less smooth for higher ones. Mathematically, it is easy to understand, why the first method produces vanishing moduli near the surface of the pile. Both stresses and strains go to zero there, but while we have a pretty accurate method for measuring stresses, our strain results will have larger numerical errors (strains requiring the direct or indirect numerical calculation of derivatives). These errors produce non-zero denominators in (22), leading to vanishing moduli. Using Eq. 19 to fit compliances, we have stresses in the numerator and the denominator, so the vanishing of stresses will not immediately lead to vanishing elastic constants. But what is physically correct? While the stress and strain components all should go to zero near the surface, there is no reason for the elastic coefficients to do so. All that is needed for plastic behaviour is that the ratio between shear and normal stresses exceeds a certain threshold, and indeed in the elastoplastic theory [1,18], the elastic moduli are assumed to be constant (and asymptotically large). So it appears that the results obtained fitting compliances are reliable. The fact that the smoothness of the curves is better using compliances near the bottom of the pile and better using moduli near its top, suggests that the best pragmatic engineer-like approach will be to average the results of the two methods.

Before considering the interesting differences observed for the shear modulus in the isotropic and anisotropic models, let us remark that we use a particle Young's modulus of $Y = 10^7$ N/m and that the scale of the *measured* elastic modulus of the sand pile is approximately $E = 10^6$ N/m, i.e. one order of magnitude smaller. This means, the simulated sand pile is softer by about one order of magnitude than its individual particles indicating a decrease in the stiffness of the sand piles. From this, we may conclude that *sound velocities* in the sand pile, a topic concerning the dynamic behaviour of granular aggregates that has raised some interest recently [43,44] should be significantly lower than sound velocities in the bulk material. Of course, we cannot make statements about the *S mode* discussed in [43] on the basis of a simple elastic constant calculation, this would rather require dynamical simulations or measurements as the ones done in [44]. But we can make assertions about the *E mode*, describable by a continuum limit and in the elastic region of the pile governed by the pertinent elastic moduli. So we would expect a quasi-longitudinal mode, governed essentially by the bulk modulus, and a quasi-transversal one, governed mostly by the shear modulus. (In an isotropic continuum, we could leave out the words "quasi", "essential", and "mostly" in the preceding sentence, because the sound velocities are given by $c_L = \sqrt{K/\rho}$ and $c_T = \sqrt{G/\rho}$ there.)

This then takes us to the most interesting part of the comparison, the fact that there *is* a substantial difference in the shear moduli for the two calculations (which persists if we do the anisotropic calculation via fitting of moduli instead of compliances): the shear modulus has a maximum near the centre line of the pile in the bottom layers of the pile according to the calculation assuming isotropic elasticity, but it has a minimum, if cubic anisotropy is assumed. Note first that if everything is done properly, it is logically impossible for
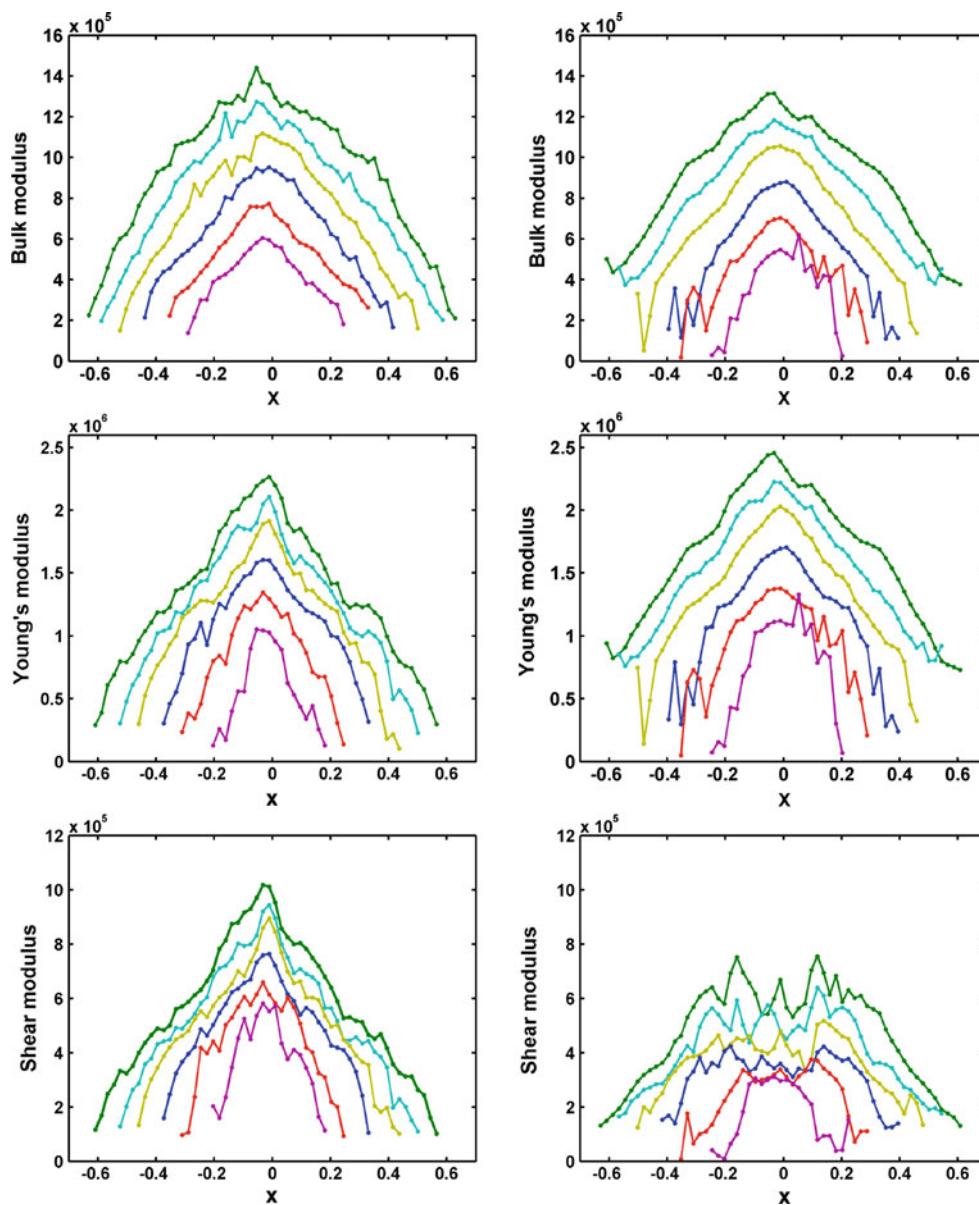
Fig. 4 Effective material properties from simulations of sand piles poured from a point source. *Left* moduli calculated assuming isotropic elasticity, via minimization of the sum S' (21), using a single point ($m = 1$) at the centre of each RVE. *Right* moduli calculated assuming linear elasticity with cubich anaisotropy, via minimization of $\tilde{S}$ (18), using 5 points ($m = 5$) near the centre of each RVE. All moduli are given in N/m. Layer heights are as in Fig. 2

results from the isotropic calculation to be right if those from the anisotropic one are wrong, because the anisotropic case contains the isotropic one as a limiting case. If an isotropic model gives the true behaviour, the anisotropic one must reproduce this. Hence, unless both results are wrong, the anisotropic one must be correct and this proves that elastic anisotropy does have some important consequences in our sand piles. There are some directions in the material, along which it shows very weak resistance to shear.

To explain this qualitatively, we combine a prior result with observations of the dynamics during the pouring process. As reported in [41], we found the mass density ρ inside a sand pile accumulated via a wedge sequence to be *higher* below its tip in the region of *reduced* pressure p than in its surroundings, which is quite counterintuitive. One would rather expect the density to decrease when the pressure decreases, because $dp/d\rho < 0$ should result in a negative compressibility, and a negative compressibility means mechanical instability plus a negative bulk modulus, which we do not measure. In fact, what we see here, is that the "constitutive equation" or equation of state involves non-uniqueness of the dependence $p(\rho)$, as we can, by reducing

the gravity level, diminish both the pressure and the density, until we have the same density at the centre of the pile as we had off-centre before gravity reduction, but we will have it at a much lower pressure. This is akin to the example of the ferromagnet invoked in the introduction, where we can have different magnetizations at the same external field, depending on the history of magnetization. In the sandpile, we can have different pressures at the same density, depending on how this density was arrived at. On the other hand, in sand piles grown layer by layer, the density is constant everywhere except close to the surface. Moreover, the dynamics of formation of a pile produced via the wedge sequence is rather violent—almost all of the time, there are avalanches, leading to a selection of the angle of repose, whereas for a pile generated via a layered sequence, growth is relatively smooth, and by adapting the speed of length reduction of the line source, any slope angle between zero and the maximum angle of repose can be created. Besides selecting a definite angle of repose, the avalanche dynamics of sand piles obtained from a point source leads to the emergence of force chains. These chains entail arching, which is, generally speaking, the explanation for the pressure minimum.

But we can form a much more detailed physical picture of how this minimum arises. We may visualize the continuing sequence of particles falling from the point source as a tapping experiment for the particles below the surface, because there will be fluctuations and intermittency in the momentum transfer to the particles that have already settled down. In experiments, tapping is often done from below, but that is more or less for practical reasons. If the flowing sand itself is at the origin of fluctuating momentum transfer, there is no reason why tapping could not happen from above. It is known that tapping leads to compaction. So the material below the emerging arch compactifies, which leads to an increased density and chains of jammed particles but also a lowered pressure underneath, because these chains will carry a larger percentage of the forces. In additon, a layer of loosely packed material should be produced just below the arch(es). The bulk modulus will hardly be affected by this. However, the shear modulus along this layer should be greatly reduced. This is a way to rationalize the appearance of a minimum in the shear modulus at the centre of the pile, but clearly the situation calls for a more detailed investigation in terms of a model taking into account the most general linearly elastic configuration, i.e., starting from the full expression (16) or its analog in terms of compliances. Such an endeavor is beyond the scope of the present paper.

6 Distribution of stress and strain invariants

We plot in Fig. 5 the trace of the (negative) incremental stress tensor as a function of the trace of the (negative) strain tensor
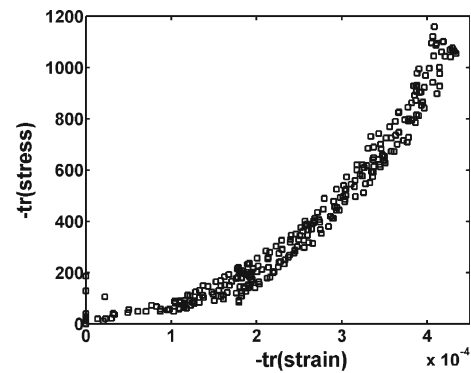
Fig. 5 Correlation between trace of the incremental stress tensor (in N/m) and trace of the strain tensor for wedge-sequence sand piles

for sand piles created from a point source. The graph shows that the behaviour is nonlinear. The left part of the graph (with strains below 2×10^{-4}) corresponds to the points that are close to the surface of the sand pile.

The slope of this graph is proportional to the differential bulk modulus; we observe that it decreases smoothly near the surface suggesting a smooth transition from elastic to plastic behaviour rather than a discontinuous one. What is interesting about this graph (though not difficult to understand) is that we have (roughly) linear elastic behaviour for large strains (between 3×10^{-4} and 4×10^{-4}) and stresses and nonlinear behaviour announcing the transition to plastic behaviour for smaller strains, contrary to what one sees in solid state mechanics, where plastic behaviour is a consequence of large loads. Of course, this is due to the non-cohesive nature of the granular medium. Under compressive external load the pile behaves mostly elastic, but when this load becomes small or negligible, the lack of attractive interaction between the particles makes itself felt, the aggregate starts to act like an isostatic network [45], which is almost flexible, and hence plastic.

Similar behaviour was observed in the analytical approach [1] for sand piles obtained by Didwania, Cantelaube, and Goddard as they assumed linear elastic behaviour near the centre and plastic behaviour closer to the surface of the sand pile. For simplicity, they considered constant (asymptotically large) elastic coefficients in the whole elastic domain of the pile. As we have discussed in another paper [41], the elastoplastic approach produces a decent approximation for the pressure along the bottom layer of the pile. Our results in the present paper demonstrate that the stress fields at the interior of the sand pile are not as well described by this simplified approach, due to an inhomogeneous distribution of elastic properties.

7 Conclusions

We have performed simulations of two-dimensional granular aggregates consisting of convex polygons and measured

microscopic force distributions of the resulting "sand piles". Via averaging over representative volume elements, for which a sufficient size was determined to contain 100–200 particles, we have determined stress, strain and fabric distributions. To obtain a measure for strain, the sand pile was allowed to relax under reduction of gravity. While it may be difficult or impossible to determine the strain tensor in an experimental sand pile, its estimation from simulations is feasible. We define the strain with respect to a hypothetical reference state at zero gravity. This reference state may be approximated from the static pile obtained in a simulation by slowly changing gravity and following the particle trajectories during the ensuing load change. Then it is easy to compute the macroscopic strain tensor by averaging over an RVE. It turns out that the size of the RVE we need for converged strain tensors is the same as for stress tensors. For total strains, the procedure gives no more than a rough estimate, which is best for the u_{yy} component. For incremental strains, it allows their precise measurement and a zero-strain reference state is not needed in that case.

We find that the vertical normal strain u_{yy} is not only minimum at the bottom layer, but also in higher layers of the sand piles constructed by a wedge sequence. However, it disappears in layers near the tip of the pile. A similar vertical normal strain minimum was not obtained in piles poured from a line source, which suggests that the construction history affects the strain distribution under a sand pile in a similar way as it does for the stress distribution.

In the next step, we determine elastic constants for sand piles poured from a point source using incremental stresses and strains and assuming Hooke's law throughout the pile. Comparing an isotropic model with a model invoking cubic anisotropy we notice that elastic constants such as the bulk modulus and Young's modulus are hardly affected by the model choice and can thus be measured with some reliability. Consequences for sound propagation in granular materials are briefly discussed and support earlier work [44]. On the other hand, results for the shear modulus are strongly model dependent, meaning that isotropic elasticity cannot work. We offer a preliminary explanation for the minimum in the shear modulus obtained from an anisotropic model. Whether this explanation indeed contains the essential physics is a question to be decided by more research in the future.

For the time being, we present the following physical picture explaining the appearance of a pressure minimum in sand piles poured from a point source and its absence in sandpiles constructed layerwise. In the latter case, the impact of new particles is relatively smoothly distributed along the top layer of the growing pile; each layer can relax mechanically before the next one is built, avalanches are absent. On the other hand, when particles arrive from a point source, the central part of the pile is persistently bombarded with a fluctuating stream of particles, which is akin to an aggregate being "tapped from

the top". This leads to local compactification and arching following the emergence of bridges of jammed particles. These support force chains leading to a reduction of pressure below them. This way the appearance of a density maximum and a pressure minimum at the same time, otherwise counterintuitive, becomes understandable.

Finally, we determine the correlation between invariants of the stress and strain tensors for a change in gravity of about 15%; the observed stress and strain relation is nonlinear, due to the distribution of local properties varying from the centre to the surface of the pile. While we have almost linear elastic behaviour near the centre of the pile, there is softening of the elastic constants announcing the transition to plastic behaviour near the surface of the pile. This behaviour is mimicked by the model given by Cantelaube et al. [1] (but without a change in elastic constants). We observe that the macroscopic tensors stress and fabric are not collinear in the sand pile, which is in line with our observations about the necessity of an elastically anisotropic description.

Appendix: Calculation of contact forces

In principle, the contact force should be computed from the deformation of two colliding particles and their elastic properties. As discussed in the body of the paper, this is not practical. Instead particles are allowed to overlap without shape change, but a repulsive force is introduced that increases strongly with increasing overlap of a pair of particles. Figure 6 visualizes the geometrical elements that are relevant to the calculation. Due to the convexity of overlapping particles, their boundaries will intersect in exactly two points c_1 and c_2, as soon as there is a finite overlap area. The straight line joining these points is the contact line, used to define a normal direction $\mathbf{n}_\perp$ and a tangential direction $\mathbf{n}_\parallel$ as well as the point where contact forces act—for this the midpoint $\mathbf{s}_{ij}$ of the contact line is chosen. As we assume equal density for all particles, their masses m_i and m_j are directly proportional to their areas. The contact point $\mathbf{s}_{ij}$ is also needed in the definition of the branch vectors $\mathbf{r}_i$ and $\mathbf{r}_j$ which connect the centres of mass of the particles to it. The overlap area A is calculated using the surveyor's formula for the inner polygon containing the corners c_1 and c_2. Dynamical quantities needed in the force calculation are the particle velocities $\mathbf{v}_i$ and $\mathbf{v}_j$ and the angular frequencies of their rotation, ω_i and ω_j.

First we define a few quantities needed in the calculation. The *characteristic* or *contact length* is given by $l = \frac{r_i r_j}{r_i + r_j}$, where $r_i = |\mathbf{r}_i|$, $r_j = |\mathbf{r}_j|$ (so it is *not* the length of
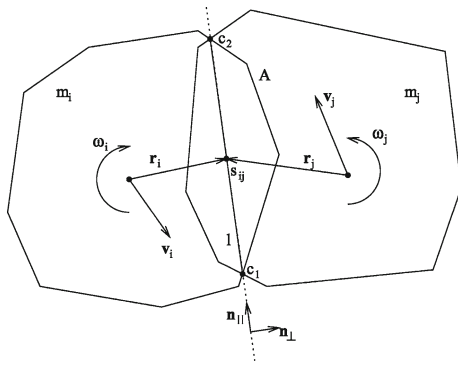
Fig. 6 Illustration of geometrical and dynamical quantities used in the calculation of two colliding particles. The size of the overlap area is strongly exaggerated

the contact line). This is half the harmonic mean of the branch vector lengths corresponding to the common contact of the two particles. If one of the particles is much smaller than the other, l becomes equal to its branch vector length. This choice of a characteristic length accounts for the fact that the same elastic displacement is much more easily imposed on a large body than on a small one, or to put it differently that short springs are stiffer than long ones. Next, we introduce a reduced mass via $m_\perp = \frac{m_i m_j}{m_i + m_j}$, and a "tangential" mass

$$m_{||} = \cfrac{1}{\frac{1}{m_i} + \frac{1}{m_j} + \frac{r_i^2}{I_i} + \frac{r_j^2}{I_j}},$$

where I_i and I_j are the moments of inertia of the particles with respect to their centres of mass [see also (1)], calculable from their polygonal shape assuming homogeneous mass density. The tangential velocity of one particle referred to the other is $v_{||} = (\mathbf{v}_1 - \mathbf{v}_2 + \mathbf{r}_1 \times \boldsymbol{\omega}_1 - \mathbf{r}_2 \times \boldsymbol{\omega}_2)\mathbf{n}_{||}$. We define a penetration depth using the overlap area A and the characteristic length l: $d_{\text{eff}} = A/l$. This depth is essentially proportional to the overlap area, as the characteristic length changes very little during a collision. With these definitions, the contact force consists of three contributions.

(i) An elastic repulsive force normal to the contact length:

$$F_\perp = Y d_{\text{eff}} = Y \frac{A}{l} \,.$$

Here, the particle Young's modulus Y is introduced.

(ii) A dissipative normal force to account for the fact that collisions are almost always inelastic: This force is constructed in two steps. First, we set

$$D_\perp^* = \gamma \sqrt{Y m_\perp} \dot{d}_{\text{eff}} = \gamma \sqrt{Y m_\perp} \frac{\Delta A}{l \Delta t},$$

where the second formula follows from the assumption that l is constant during the collision. γ is a damping

coefficient. Now it can happen that $\left| D_\perp^* \right|$ becomes larger than $|F_\perp|$, which is not a problem when the two particles approach each other. But if this occurs while they move away from each other, then the resulting force will be attractive which is unphysical. Hence the dissipative part of the normal force is set according to the following rule

$$D_\perp = \begin{cases} D_\perp^* & \text{on approach} \\ \max(D_\perp^*, -F_\perp) & \text{on separation} \end{cases}.$$

(iii) A tangential friction force $F_{||}$, following the work of Cundall and Strack [32]: To be able to model Coulomb friction, we use the following algorithmic procedure. Whenever two particles touch, an imaginary spring is attached to the contact point. This spring is elongated during the continuing sliding motion of the particles alongside each other and a restoring force starts to build up. Of course, this force cannot become arbitrarily large, so the spring is not elongated any further, when the maximum force allowed by the static friction coefficient has been reached, instead the spring is pulled along the contact line. Clearly, the tangential force does not *have* to reach the maximum value $\mu F_\perp$, because it acts to reduce $v_{||}$, and once the relative tangential motion of the two particles stops, the spring is also not elongated any further. At initiation of a new contact, we set $F_{||}(0) = 0$ and afterwards, the tangential force evolves according to

$$F_{||}^*(t + \Delta t) = \min \left(F_{||}^*(t) + \frac{2}{7} Y v_{||} \Delta t, \; \mu F_\perp(t) \right),$$

where μ is the static friction coefficient, and the factor $\frac{2}{7}$ is adapted to Hertzian stress for spherical particles. For a sliding contact, μ should be replaced by the dynamic friction coefficient, which in our simulations is taken equal to the static coefficient. This allows us to get around the necessity of deciding whether a contact is sliding or not (which is nontrivial, as the exact value zero of the velocity is numerically infrequent). In order to avoid or reduce spurious oscillations of the tangential velocity, a viscous damping term is introduced for the tangential force similar to the procedure used in the calculation of the normal force. Setting

$$D_{||} = v_{||} \sqrt{\frac{2}{7} Y m_{||}},$$

we compute the total tangential force as

$$F_{\parallel}^*(t + \Delta t) = \pm\min\left|F_{\parallel}^*(t) + \frac{2}{7}Yv_{\parallel}\Delta t + D_{\parallel}\right|,$$

$$|\mu F_{\perp}(t)|,$$

with the sign chosen appropriately, so the force will always be opposite to the relative tangential motion of the two particles.

In total, three parameters enter the force model; these are the particle Young's modulus Y, the phenomenological viscosity γ, and the friction coefficient μ. The particle Young's modulus is a phenomenological coefficient, too, since it may differ by a (small) factor from the true bulk Young's modulus, given that the normal elastic displacement is assumed proportional to, but not necessarily equal to, A/l.

Advantages of the described modeling procedure are that a particle sliding with a small velocity on a substrate (for which another big particle may serve) will not commence continuous oscillations (it would do so, if the friction force were simply modeled as $\mu F_{\perp}$) and that a particle is able to come to rest on an inclined plane, both features that our force model should have in the interest of realism.

References

1. Didwania, A.K., Cantelaube, F., Goddard, J.D.: Static multiplicity of stress states in granular heaps. Proc. R. Soc. Lond. A **456**, 2569–2588 (2000)
2. Wittmer, J.P., Cates, M.E., Claudin, P.: Stress propagation and arching in static sand piles. J. Phys. I France **7**, 39–80 (1997)
3. Hummel, F.H., Finnan, E.J.: The distribution of pressure on surfaces supporting a mass of granular material. Proc. Instn. Civil Eng. **212**, 369–392 (1921)
4. Jotaki, T., Moriyama, R. : On the bottom pressure distribution of the bulk materials piled with the angle of repose. J. Soc. Powder Techn. Jpn. **16**, 184–191 in Japanese (1979)
5. Brockbank, R., Huntely, J.M., Ball, R.: Contact force distribution beneath a three-dimensional granular pile. J. Phys. II (France) **7**, 1521–1532 (1997)
6. Vanel, L., Howell, D., Clark, D., Behringer, R.P., Clement, E.: Memories in sand: experimental tests of construction history on stress distributions under sandpiles. Phys. Rev. E **60**, R5040 (1999)
7. Wittmer, J.P., Cates, M.E., Claudin, P., Bouchaud, J.-P.: An explanation for the stress minimum in sand piles. Nature **382**, 336–338 (1996)
8. Smid, J., Novosad, J.: Pressure distribution under heaped bulk solids. In: Particle Technology: Proceedings of the Powtech Conference. Institution of Chemical Engineers, Rugby, D**3**V, pp. 1–12 (1981)
9. Zuriguel, I., Mullin, T., Rotter, J.M.: Effect of particle shape on the stress dip under a sandpile. Phys. Rev. Lett. **98**, 028001 (2007)
10. Zuriguel, I., Mullin, T.: The role of particle shape on the stress distribution in a sand pile. Proc. R. Soc. A **464**, 99–116 (2008)
11. Matuttis, H.-G.: Simulation of the pressure distribution under a two dimensional heap of polygonal particles. Granular Matter **1**, 83–91 (1998)
12. Matuttis, H.-G., Luding, S., Herrmann, H.J.: Discrete element simulations of dense packings and heaps made of spherical and non-spherical particles. Powder Technol. **109**, 208–292 (2000)
13. Luding, S.: Stress distribution in static two-dimensional granular model media in the absence of friction. Phys. Rev. E **55**, 4720–4729 (1997)
14. Liffman, K., Chan, D.Y.C, Hughes, B.D.: On the stress depressions under a sand pile. Powder Technol. **78**, 263–271 (1994)
15. Liffman, K., Nguyen, M., Metcalfe, G., Cleary, P.: Forces in piles of granular material: an analytic and 3D DEM study. Granular Matter **3**, 165–176 (2001)
16. Li, Y.J., Xu, Y., Thornton, C.: A comparison of discrete element simulations and experiments for 'sand piles' composed of spherical particles. Powder Technol. **160**, 219–228 (2005)
17. Zhao, Y.C., Xu, B.H., Zou, R.P., Yu, A.B., Zulli, P.: Stress distribution in a sand pile formed on a deflected base. Adv. Powder Technol. **14**, 401–410 (2003)
18. Cantelaube, F., Goddard, J.D.: Elastoplastic arching in 2D granular heaps. In: Behringer, R.P., Jenkins, J.T. (eds.) Powders and Grains, pp. 231–234. Balkema, Rotterdam (1997)
19. Bouchaud, J.-P., Cates, M.E., Claudin, P.: Stress distribution in Granular media and nonlinear wave equation. J. Phys. I (France) **5**, 639–656 (1995)
20. Tejchman, J., Wei, W.: E-Calculations of stress distribution under prismatic and conical sand piles within hypoplasticity. Granular Matter **10**, 399–405 (2008)
21. Claudin, P., Bouchaud, J.-P., Cates, M.E., Wittmer, J.: Models of stress fluctuations in granular media. Phys. Rev. E **57**, 4441 (1998)
22. Lee J.H.I.K.: Proceedings of the 1st Australia New Zealand Conference on Geomechanics, vol. **1**, Melbourne, p. 291 (1971)
23. Matuttis, H.-G.: Simulation of the pressure distribution under a two-dimensional heap of polygonal particles. Granular Matter **1**, 83–91 (1998)
24. Jean, M., Moreau, J.J.: Unilaterality and friction in the dynamics of rigid body collections. In: Proceedings of Contact Mechanics International Symposioum, Presses Polytechniques et Universitaires Romandes, Lausanne, pp. 31–48 (1992)
25. Moreau, J.J.: Some numerical methods in granular dynamics. In: Powders & Grains 93. Balkema, Rotterdam, p. 227 (1993)
26. Jean, M.: The non-smooth contact dynamics method. Comput. Methods Appl. Mech. Eng. **177**, 235–257 (1999)
27. Alder, B.J., Wainwright, T.E.: Studies in molecular dynamics. I. General method. J. Chem. Phys. **31**, 459 (1959)
28. Lubachevsky, B.D.: How to simulate billiards and similar systems. J. Comp. Phys. **94**, 255–283 (1991)
29. Gear, C.W.: Numerical Initial Value Problems in Ordinary Differential Equations. Prentice-Hall, Englewood Cliffs (1971)
30. Schinner, A.: Ein Simulationssystem für granulare Aufschüttungen aus Teilchen variabler Form. PhD thesis, Univ. Magdeburg (2001)
31. Schinner, A.: Fast algorithms for the simulation of polygonal particles. Granular Matter **2**, 35 (1999)
32. Cundall, P.A., Strack, O.D.L.: A discrete numerical model for granular assemblies. Géotechnique **29**, 47–65 (1979)
33. Luding, S.: Micro-macro transition for anisotropic, frictional granular packings. Int. J. Sol. Struct. **41**, 5821–5836 (2004)
34. Bagi, K.: Stress and strain in granular assemblies. Mech. Mater. **22**, 165–177 (1996)
35. Satake, M.: Three-dimensional discrete mechanics of granular materials. In: Fleck, N.A., Cocks, A.C.E. (eds.) IUTAM Symposium on Mechanics of Granular and Porus Materials, pp. 193–202. Kluwer, Dordrecht (1997)
36. Cambou, B., Chaze, M., Dedecker, F.: Change of scale in granular materials. Eur. J. Mech. A/Solids **19**, 999–1014 (2000)

37. Goddard, J.D.: Continuum modeling of granular assemblies. Physics of Dry Granular media. In: Herrmann, H.J., Hovi, J.P., Luding, S. (eds.) pp. 1–24. Kluwer, Dordrecht (1998)

38. Cowin, S.C.: A simple theory of instantaneously induced anisotropy. Micromecanics of granular Materials. In: Jenkins, J.T., Satake, M. (eds.) pp. 71–80. Elsevier, Amsterdam (1988)

39. Luding, S. : Micro-Macro Models for Anisotropic Granular Media. In: Vermeer, P.A., Ehlers, W., Herrmann, H.J., Ramm, R. (eds.) Modelling of Cohesive-Frictional Materials, pp. 195–206. Leiden A.A., Balkema (2004)

40. Lätzel, M., Luding, S., Herrmann, H.J.: Macroscopic material properties from quasi-static, microscopic simulations of a two-dimensional shear-cell. Granular Matter **2**, 123–135 (2000)

41. Roul, P., Schinner, A., Kassner, K.: Micro and macro aspects of the elastoplastic behaviour of sand piles. In: Bertram, A., Tomas, J. (eds.) Micro-Macro-Interactions in Structured Media and Particle Systems, pp. 207–219. Springer, Berlin (2008)

42. Landau, L.D., Lifshitz, E.M.: Theory of Elasticity (Vol. **7** 3rd edn.). Butterworth-Heinemann, Oxford (1986)

43. Jia, X., Caroli, C., Velicky, B.: Ultrasound propagation in externally stressed granular media. Phys. Rev. Lett. **82**, 1863–1866 (1999)

44. El Shourbagy, S.A.M., Okeda, S., Matuttis, H.-G.: Acoustic of sound propagation in granular materials in one, two, and three dimensions. J. Phys. Soc. Jpn. **77**, 034606 (2008)

45. Moukarzel, C.F.: Isostatic phase transition and instability in stiff granular materials. Phys. Rev. Lett. **81**, 1634–1637 (1998)